# An Improvement on Analytic Accuracy of Circular Groove Guide

Hong-Sheng Yang, *Senior Member, IEEE*, and Yong Liu

***Abstract*—In this paper, an $N$th order approximate eigenequation of circular groove guide is presented. Using the sixth order approximate results, some propagation properties of the $TE_{11}^{(1)}$ mode of circular groove guide are recalculated. The results are more accurate than before and in good agreement with the measurements.**

***Index Terms*—Attenuation coefficient, circular groove guide, cutoff wavelength, power capacity.**

## I. Introduction

CIRCULAR groove guide is one type of groove guides and was first put forward in 1989 [1]. It has many advantages, such as low loss, high power capacity, low dispersion, large dimensions, single mode operating, etc. [1], [2].

The second order approximate eigenequation of the $TE_{11}^{(1)}$ mode of circular groove guide has been derived before [2]. In paper [2], field components are written in series forms. The series are truncated to polynomial when calculating. Meanwhile, the truncated error is introduced to results. The more terms the polynomial adopts, the less error arises.

The first order approximation is the simplest. Under this circumstance, all field components are expressed as monomial and the truncated error is the largest one. When the order of approximation is increasing to a certain number, the truncated error is always acceptable.

In the past, only the first and second order approximate results were available [2]. Now, this paper presents the $N$th order approximate eigenequation in Section II. Some important properties of the $TE_{11}^{(1)}$ mode of circular groove guide are given in Section III based on the sixth order approximate results. Conclusion is in Section IV.

## II. The Eigenequation

The cross section of circular groove guide is shown in Fig. 1.

It is assumed that the direction of wave propagation is $z$ direction. The guide can be divided into three regions, i.e., the central groove region designed by $A$ which has a circular boundary with diameter $2a$ and two evanescent side regions designated by $B$ and $B'$. The spacing between the two parallel plates is $2c$. According to that geometrical shape, we take cylindrical coordinate in region $A$ and Cartesian coordinates in region $B$ and $B'$. They have the same $z$-axis.

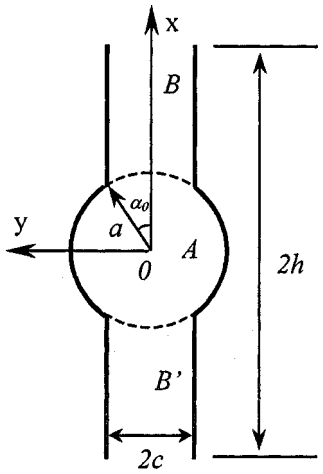


Fig. 1. Cross section of circular groove guide.

The longitudinal field components of the $TE_{pq}^{(r)}$ mode in three regions are written below

$$H_{zA} = \sum_p H_p J_p(k_c\rho)\sin(p\alpha) \tag{1}$$

$$H_{zB} = \sum_r B_r k_c^2 \sin(k_{yr}y)\exp[-k_{xr}(x-x_0)] \tag{2}$$

$$H_{zB'} = \sum_r B_r k_c^2 \sin(k_{yr}y)\exp[k_{xr}(x+x_0)] \tag{3}$$

where $p = 1, 3, \ldots, r = 1, 3, \ldots$. $H_p$, and $B_r$ are amplitude coefficients in region $A$, $B$, and $B'$, respectively. $k_c$ is the cutoff wavenumber. $J_p$ is the $p$ order Bessel function. $jk_{xr}$ and $k_{yr} = r\pi/2c$ are wavenumbers in $x$ and $y$ direction respectively. $x_0$ is the scale value of $x$ coordinate at the arc boundary between region $A$ and $B$.

The boundary conditions between region $A$ and $B$ are given by following expressions

$$H_{zA} = H_{zB} \qquad (\rho = a,\ 0 \le \alpha \le \alpha_0), \tag{4}$$

$$E_{\alpha A} = \begin{cases} -E_{xB}\sin\alpha \\ \quad +E_{yB}\cos\alpha & (\rho = a,\ 0 \le \alpha \le \alpha_0), \\ 0 & (\rho = a,\ \alpha_0 < \alpha \le \pi/2). \end{cases} \tag{5}$$

Then, we get the eigenequation of the $TE_{pq}^{(r)}$ mode with the $N$th order approximation

$$\det(\mathbf{E}_{N\times N}) = 0 \tag{6}$$

Manuscript received June 28, 2001; revised November 13, 2001. This work was supported by the National Science Foundation of China. The review of this letter was arranged by Associate Editor Dr. Ruediger Vahldieck.

The authors are with the Department of Electronic Engineering, National Key Laboratory of Millimeter Waves, Southeast University, Nanjing, China (e-mail: hsyang@seu.edu.cn).

Publisher Item Identifier S 1531-1309(02)01821-4.

where

$$\mathbf{E} = \mathbf{TW} - A_3 \frac{\pi}{4} u\mathbf{U}$$

$$\mathbf{T}_{N\times N} = \sum_{m=1}^{N}\sum_{n=1}^{N} T_{mn} = \sum_{m=1}^{N}\sum_{n=1}^{N} R[p+2(m-1),\, r+2(n-1)]$$

$$\mathbf{W}_{N\times N} = \sum_{m=1}^{N}\sum_{n=1}^{N} W_{mn} = \sum_{m=1}^{N}\sum_{n=1}^{N} A_1[p+2(n-1),\, r+2(m-1)] \cdot J_{p+2(n-1)}(u)$$

$$\mathbf{U}_{N\times N} = \sum_{m=1}^{N}\sum_{n=1}^{N} U_{mn} = \sum_{m=1}^{N}\sum_{n=1}^{N} J'_{p+2(m-1)}(u)\delta_{mn},$$

$$\delta_{mn} = \begin{cases} 1 & (m=n) \\ 0 & (m\neq n) \end{cases}$$

$$R(p,\, r) = rMA_2(p,\, r) - v_r A_1(p,\, r)$$

$$u = k_c a, \quad rM = k_{yr} a, \quad v_r = k_{xr} a$$

$$A_1(p,\, r) = \int_0^{\alpha_0} \sin(p\alpha)\sin(rM\sin\alpha)\cos\alpha\, d\alpha$$

$$A_2(p,\, r) = \int_0^{\alpha_0} \sin(p\alpha)\cos(rM\sin\alpha)\sin\alpha\, d\alpha$$

$$A_3 = \frac{c}{2a}, \qquad \alpha_0 = \sin^{-1}\frac{c}{a}.$$

## III. Propagation Characteristics of the $TE_{11}^{(1)}$ Mode

The first root of eigenequation (6) is the eigenvalue of $TE_{p1}^{(r)}$ mode. When $p = 1$ and $r = 1$ the first eigenvalue is the cutoff numbers of $TE_{11}^{(1)}$ mode.

### A. The Cutoff Wavelength of the $TE_{11}^{(1)}$ Mode

While solving the eigenequation of different order approximation, we get the corresponding eigenvalues. They all vary with the change of $c/a$. Fig. 2 shows that $\lambda_c/2a$ versus $c/a$ in various approximation. It is found that with the increasing order of approximation the curves converge.

The sixth order approximate results agree better with the experimental data than before [2]. For example, when the operating wavelength is 6.09 mm, the sixth order approximate guide wavelength is 6.195 mm. It is closer to the experimental value 6.188 mm than the foregoing value 6.199 mm.

The two ends of the curves approach to 1.706 and 2, respectively. The former $\lambda_c/2a$ is the corresponding value of the lowest mode in circular guide and the later $\lambda_c/2a$ is that of the lowest mode in parallel plate guide.

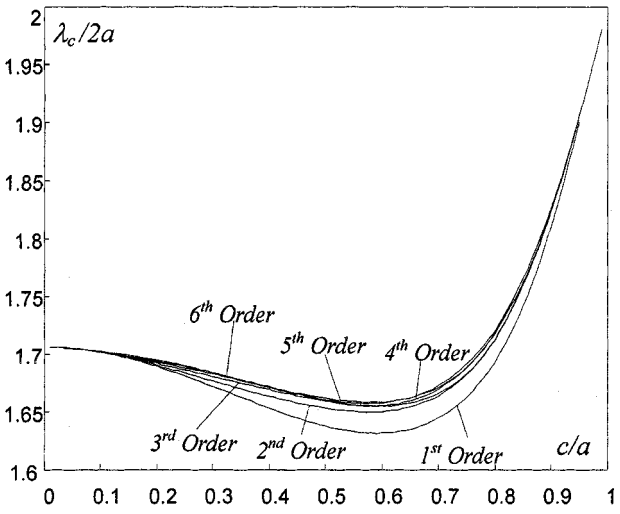


Fig. 2. Relations between $\lambda_c/2a$ and $c/a$ in various approximation.

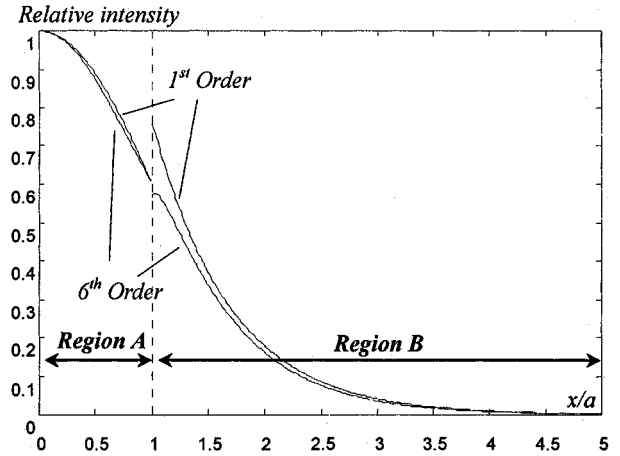


Fig. 3. $E_x$ component distribution along $x$-axis.

Based on the higher order approximate results, it is convenient to describe the field of the $TE_{11}^{(1)}$ mode accurately at any point.

Fig. 3 shows the distribution of relative intensity of $E_x$ component along the $x$-axis. In the first order approximation, there is a discontinuity at the boundary between region $A$ and $B$ (i.e., $x/a = 1$). Choi got the similar result when he analyzed the rectangular groove guide [3]. When the order of approximation increases the discontinuity trends to zero. Moreover, $E_x$ component evanesce sharply as entering region $B$. This means the field could propagate along $z$ direction in circular groove guide.

Fig. 4 shows the relative intensity of electric field and transverse field distribution in the cross section of circular groove guide. The height in the figure represents relative intensity of the field. It is found that the field is mainly contained in region $A$. The maximum intensity appears at the center of the cross section and the four corners. If the guide is fed with very large power, the breakdown of the gas will take place at one of those points first.

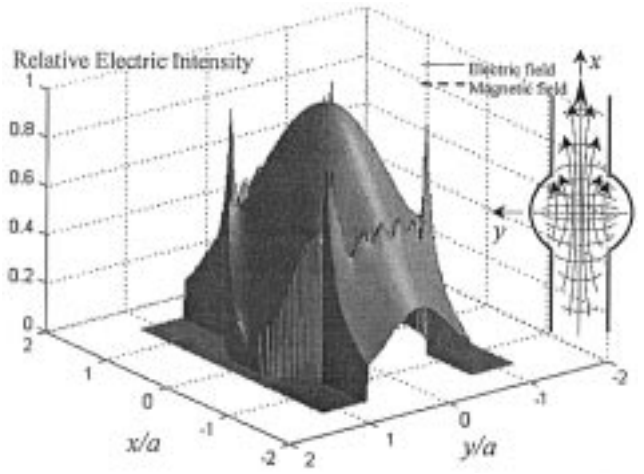


Fig. 4. Relative electric intensity and transverse field distribution of $TE_{11}^{(1)}$ mode in the cross section in the sixth order approximation.

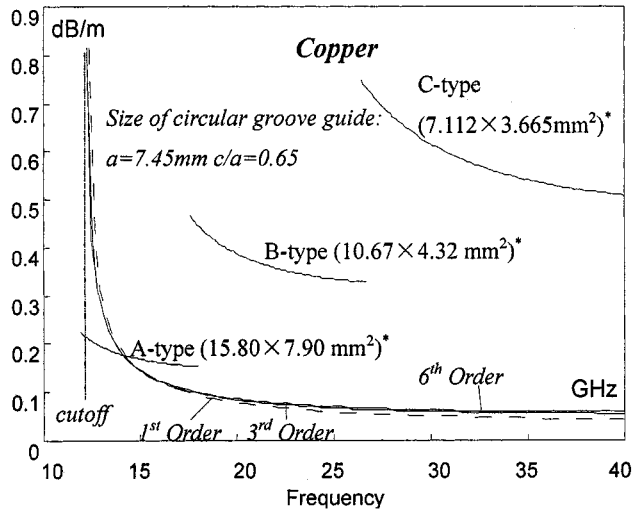


Fig. 5. Comparison of attenuation between circular groove guide and rectangular guide.

### B. Attenuation Coefficient of the $TE_{11}^{(1)}$ Mode

The loss in circular groove guide consists of two parts. One is the conductor loss on metallic wall, the other is the power radiating along the $\pm x$ directions, which is due to the finite highness $h$. Fig. 5 compares the attenuation coefficient between circular groove guide and standard rectangular guide. In addition, the curves of attenuation coefficient of circular groove guide in three different approximations are shown. It is clear that the attenuation coefficient of circular groove guide is lower than that of standard rectangular guide.

### C. Power Capacity of Circular Groove Guide

The power carried by $TE_{11}^{(1)}$ mode is calculated via the integral of the *Poynting* vector over the entire cross section.

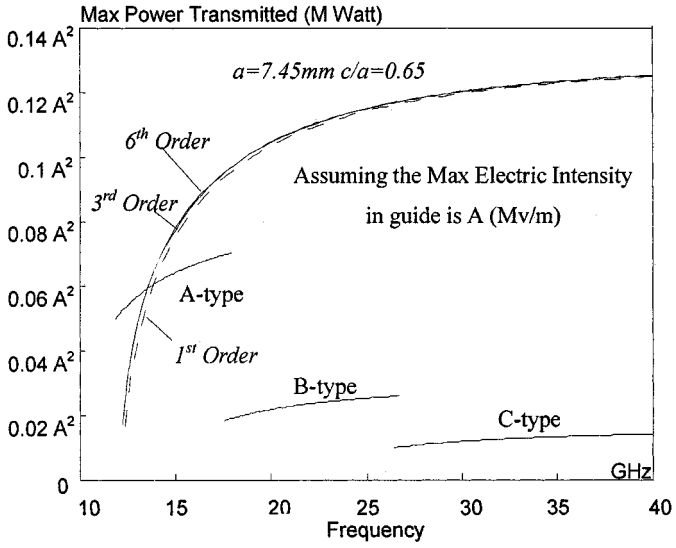


Fig. 6. Comparison of power capacity between circular groove guide and rectangular guide.

The microwave power capacity is defined as the maximal transmitted power just before the breakdown of the gas. It is assumed that the breakdown takes place at field intensity of $A$ (Mv/m) at 760 torr and specific operating frequency band.

Fig. 6 shows the comparison of power capacity between circular groove guide and rectangular guide. The cutoff parts of rectangular guide are neglected for clarity.

## IV. Conclusion

An improvement on analytic accuracy of circular groove guide has been studied. The eigenequation of the $N$th order approximation is presented. Using the sixth order approximate results some important parameters of $TE_{11}^{(1)}$ mode are recalculated, such as cutoff wavelength, field distribution, attenuation coefficient and power capacity.

This study not only provides more accurate results than before but also confirms advantages of circular groove guide again, such as low loss, large dimensions and high power handling.

## References

[1] Y. Hongsheng, M. Jianglei, and L. Zhongzuo, "A new type of groove guide," in *2nd Int. Symp. Recent Advances Microwave Tech.*, 1989, pp. 239–240.

[2] H.-S. Yang, J. Ma, and Z.-Z. Lu, "Circular groove guide for short millimeter and submillimeter waves," *IEEE Trans. Microwave Theory Tech.*, vol. 43, no. 2, pp. 324–329, Feb. 1995.

[3] Y. M. Choi and D. J. Harris, "Groove guide for short millimeteric waveguide system," *Inf. Millim. Waves, Millim. Compon. Tech.*, pt. 3.V.11, pp. 99–140, 1984.